WAVE PROPAGATION FROM COMPLEX 3D SOURCES USING THE REPRESENTATION THEOREM

Jeffry L. Stevens and Heming Xu

Science Applications International Corporation

Sponsored by the Air Force Research Laboratory

Award No. FA8718-08-C-0010

ABSTRACT

The objective of this project is to investigate generation of complex seismic waves by explosions in media with 3D heterogeneity using a method based on the exact representation theorem for propagating complex 3D source calculations to the local, regional and teleseismic distances at which they are observed. To accomplish this, we have 1) developed a new three-dimensional nonlinear finite element code CRAM3D, which incorporates all of the nonlinear material models from our well-tested axisymmetric finite difference code CRAM; and 2) developed interface code using the representation theorem to propagate the solution. The interface code uses Green's functions for full-waveform seismograms, modal surface waves and far-field body waves in plane-layered earth models external to the source region and propagates the full 3D solution to any desired location. During the past year, we have implemented a more robust algorithm in the 3D code to improve the grid stability for large grid distortions. Tensile cracking models have also been implemented and tested. As in the 2D code, CRAM3D includes gravity and so can calculate the important nonlinear effects caused by the variation of overburden pressure with depth.

Also during the past year, we implemented the representation theorem for far-field body waves. Although this is the simplest of the three Green's functions, it proved to be the most difficult to implement because it requires exact cancellation of waveforms from different parts of the grid. We reported last year that excellent agreement was obtained between solutions using the representation theorem and analytical solutions for both full-wave solutions and surface wave solutions. The far field body wave solutions (*P*, *SV,* and *SH* waves) calculated using the representation theorem algorithm are now also in very good agreement with the analytical solutions.

We performed calculations in the presence of topography and lateral elastic and nonlinear heterogeneities in order to look at the effect these variations cause on explosion-generated seismic waves. Two sets of calculations were performed in these heterogeneous structures, the first with a yield of 0.2 kt, the second with yield of 5 kt, each detonated in a spherical cavity with a radius of 5 meters. In the 5 kt explosion, the cavity radius expands to 15 meters above the cavity, 11 meters below and 13 meters to the side. Topography is implemented by gradually distributing offsets of the grid from top to bottom and heterogeneities are implemented by setting different material properties from the background properties in different areas. The results in the presence of topography and lateral heterogeneities show significant tangential wave components due to the asymmetry in the surrounding media in the near field. Nonlinear deformation and tensile cracking are shown to extend to a large distance beyond the cavity radius; about 300 meters varying with direction for the 5 kt explosion. The inelastic regions become non-symmetric, especially near the surface, in the presence of topography and heterogeneities, and cause the tangential motions. The calculations were benchmarked against the equivalent two dimensional axisymmetric calculations for the uniform model, demonstrating the proper numerical implementation of the complex nonlinear materials.

We propagated 3D calculations using the full waveform representation theorem at a local distance of 2.5km, and at a regional distance of 650 km. The results at the local distance show significant tangential motions for the heterogeneous models. For the topographic model the tangential motions are strongly direction dependent and diminish with distance. The surface wave motions are significantly modulated by the topography and lateral heterogeneities whereas the body waves are less affected by the inhomogeneities. We propagate a calculation of a 5 kt explosion at 402 m depth with variable strength across the source region to a distance of 650 km using the representation theorem. There is a strong *SH* component not present in a uniform strength calculation.

OBJECTIVES

The objective of this project is to investigate generation of complex seismic waves by explosions in media with 3D heterogeneity using a method based on the exact representation theorem for propagating complex 3D source calculations to local, regional and teleseismic distances at which they are observed.

RESEARCH ACCOMPLISHED

To accomplish the project objectives, we:

1. Developed a 3D nonlinear finite element code designed for calculation of explosions in 3D heterogeneous media with well-tested material models and including gravity;
2. Implemented interface codes using the representation theorem that propagate the numerical solution from the source region to regional and teleseismic distances;
3. Used the code to evaluate the effect of near source heterogeneity including non-linear material property variations, elastic variability and topography.

The reason that 3D calculations are important for understanding shear wave generation is that symmetry constraints imposed by 1D and 2D calculations act to suppress shear waves. To see this, consider trying to do an explosive experiment in which 2D axisymmetry is imposed. This requires that the motion generated by the explosion be identical in all horizontal directions through propagation of the shock wave, nonlinear deformation of the surrounding material, and rebound to a final state. Since the motion is never identical in all directions, shear waves will always be generated, and in fact shear waves are observed from almost all underground explosions.

An example is shown in Figure 1, which shows near-field radial velocity and displacement from the 12.5-kiloton underground explosion SHOAL, which was detonated at a depth of 370 meters in granite at a location near Fallon, Nevada on October 26, 1963. Seismic instruments were placed in boreholes at shot depth in three directions at a distance of 590 meters from the explosion (Weart, 1965). The observed ground motion was quite different in three directions each separated by about 120º. This asymmetry generates motion across the region of deformation that acts as a secondary seismic source with the form of a horizontal dipole (Stevens and Baker, 2009; Zhou and Harkrider, 1992). Note that the final displacement at station PM-1 to the southwest is negative, while the final displacement at PM-3, to the east-southeast, is positive and large indicating a permanent displacement to the east across the region south of the explosion.

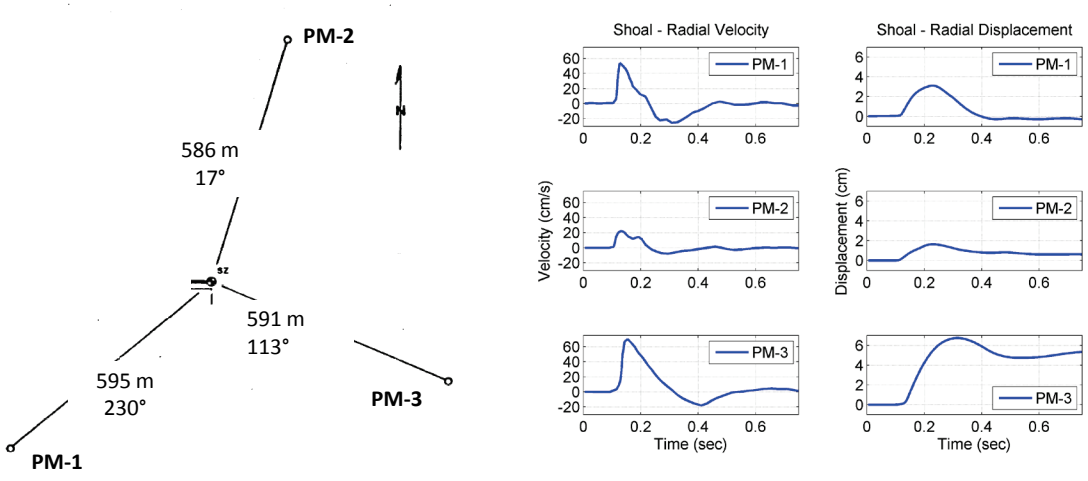

Figure 1. Radial velocity and displacement at shot level in three directions from the 12.5 kiloton underground explosion SHOAL.

The SHOAL example clearly shows substantial heterogeneity in near field motion, and in particular shows motion that differs substantially across the nonlinear region of the event. While the explosion also generates some near-field S that is visible on the vertical and tangential components (not shown), these are high frequency shear waves that may not be visible at regional and teleseismic distances. However, the heterogeneity across the entire source region generates shear waves at lower frequency corresponding to the propagation time across that region. This is

consistent with observations of Fisk (2006, 2007) and Murphy et al. (2009) of *P* and *S* corner frequencies that correspond to the P and S travel times across the source region, respectively.

It is clear that 3D effects in the source region are important and very likely ubiquitous. *SH* waves are commonly observed within a few km of explosions, too close to have been generated by (simple) conversion of vertical and radial components, and often larger than those components. Furthermore, it has not been established what impact 3D effects have on discriminants and on explosion yield estimates. It is important, therefore, to be able to model and understand how 3D source and source region heterogeneity affect the seismic wavefield, and what impact this has on parameters used for nuclear monitoring.

Source Region Calculations and Propagation Using the Representation Theorem

Our approach is to perform 3D explosion source region calculations, and then to propagate the wavefield to local, regional and teleseismic distances using layered earth Green's functions. We are interested in near-source heterogeneities in both the nonlinear and linear regimes, and therefore require both nonlinear and linear 3D codes to model the source region. In previous projects, we have used three nonlinear codes, SKIPPER, STELLAR and CRAM, and the 2D and 3D linear elastic code TRES3D. In the current project, we have developed a 3D finite element code, CRAM3D, based on material models and concepts in axisymmetric CRAM. These codes are described briefly in Table 1.

Table 1. Numerical simulation tools used in this project

Numerical Simulation Tools	
STELLAR	Eulerian finite difference code. Used to simulate the early time history of the explosion shock. It handles material strength correctly, which is difficult for an Eulerian code. Uses second order accurate Riemann solver scheme. 1D, 2D planar and axisymmetric, and 3D.
SKIPPER	One-dimensional spherically symmetric Lagrangian finite difference code. Has been used extensively for free-field explosion modeling.
CRAM	Lagrangian nonlinear finite difference code. Has been used extensively for axisymmetric explosion calculations.
CRAM3D	3D Lagrangian nonlinear finite element code developed during this project. Contains material models also used in CRAM that have been extensively tested.
TRES3D	Elastic finite difference code. 2D planar and axisymmetric, and 3D.
Elastodynamic Representation Theorem	The time dependent displacements and stresses from 3D source region calculations are saved on a monitoring surface located outside of the region of nonlinear response and/or 3D heterogeneity. A numerical implementation of the representation integral is then used to compute the corresponding far-field seismic radiation.

In the three-dimensional numerical finite difference and finite element calculations, we save displacements and stresses due to the seismic source on a monitoring surface on the boundary of a rectangle (5 planar surfaces, excluding the upper surface), and calculate Green's functions from each point on the monitoring surface to the receiver and so the synthetic seismogram at the receiver point *X* outside of the monitoring surface is obtained by integrating over the monitoring surface S_M

$$u_i = \oiint_{S_M} \left\{ G_j^i(\xi; X) * T_j^M(\xi) - u_j^M(\xi) * S_{jk}^i(\xi; X) n_k \right\} dA \qquad (1)$$

in the frequency domain, where $G_j^i(\xi; X)$ and $S_{jk}^i(\xi; X)$ are the Green's function and the stress tensor on the monitoring surface due to a unit impulsive force at *X* in direction *i*, T_j^M is the traction on the monitoring surface due to the seismic source, *u* is the displacement on the monitoring surface, and *n* is the normal to the monitoring surface. The operator * denotes convolution and the summation convention is assumed. We use Green's functions for full waveform seismograms derived from an algorithm based on the work of Luco and Apsel (1983) and Apsel and Luco (1983); modal seismograms using a technique similar to Bache et al. (1982); and far field body waves using a procedure similar to that described by Bache and Harkrider (1976). Our objective in using multiple types of Green's functions is to gain more insight into the nature of the seismic wavefield generated by the source.

Near Field Tests of the 3D Representation Theorem

Two test cases of the representation theorem in 3D are shown below. Figure 2 shows surface motion from a point explosion at 100 meters depth calculated by three different techniques: 1) wavenumber integration; 2) finite difference; 3) finite difference to the surface shown, then by the representation theorem to the receiver. Figure 3 shows the surface motion for an explosion in the same structure plus a low-velocity inclusion between the source and receiver calculated with finite difference and finite difference plus the representation theorem. In both cases, the results are nearly identical, with the largest difference being a reflected phase from the imperfect absorbing boundary in the large finite difference calculations.

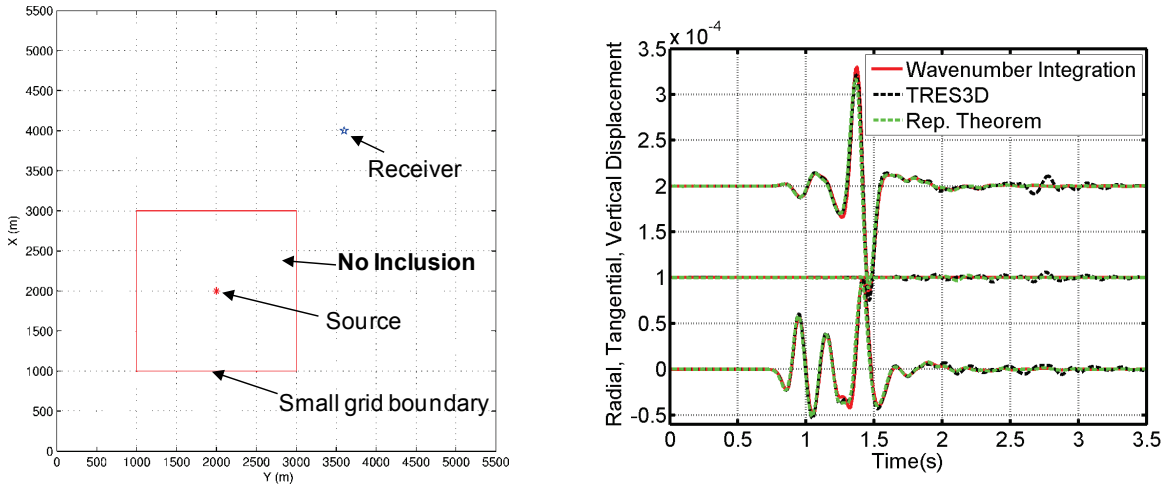

Figure 2. Calculation of surface motion from an explosion source in a plane layered structure by three different methods: wavenumber integration, finite difference and finite difference on the smaller grid plus the representation theorem.

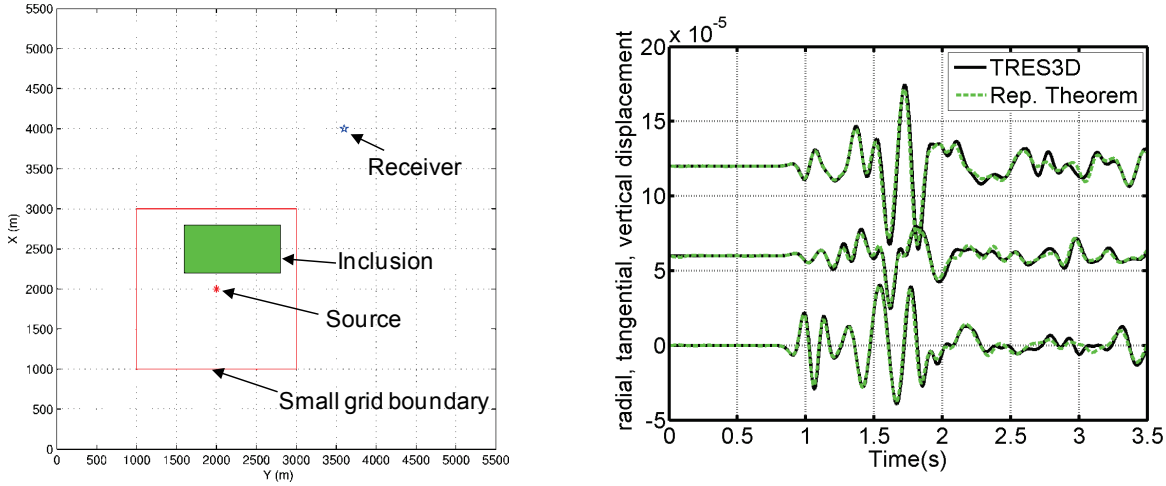

Figure 3. Calculation of surface motion from an explosion source in a plane layered structure with a low velocity inclusion by two different methods: finite difference and finite difference on the smaller grid plus the representation theorem.

CRAM 3D

CRAM 3D is an explicit three-dimensional Lagrangian finite element code designed to run on multiple processors (Stevens and Xu, 2009). For an explosion simulation, the cavity is placed near the center of the grid and is enclosed by a spider grid which facilitates applying the pressure boundary condition and rezoning elements (Figure 4). All of the well-tested nonlinear material models from CRAM 2D have been implemented. The code includes gravity and so includes the important effects that result from variation of overburden pressure with depth. The code also includes tensile cracking. Figure 5 shows a full nonlinear test calculation similar to those discussed earlier for linear elastic calculations.

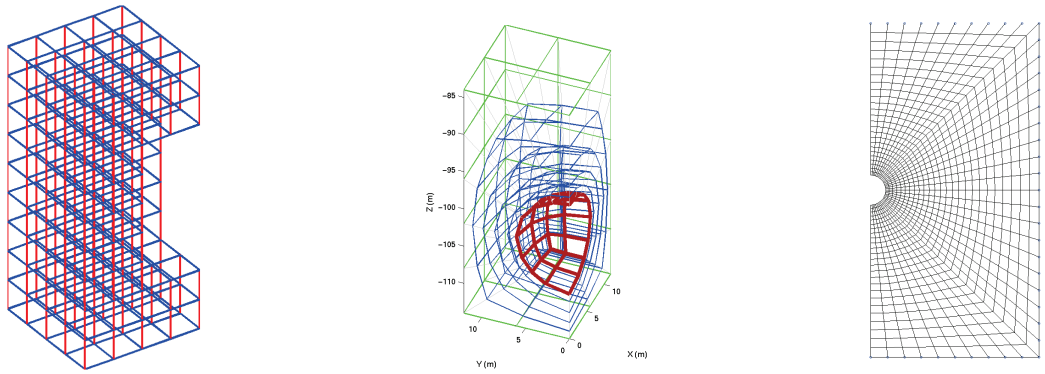

Figure 4. The CRAM 3D finite element outer grid (left) is rectangular. The inner grid (center) is shaped to match the shape of the explosion shock wave. CRAM2D uses a similar axisymmetric spider grid (right) in the region around the explosion.

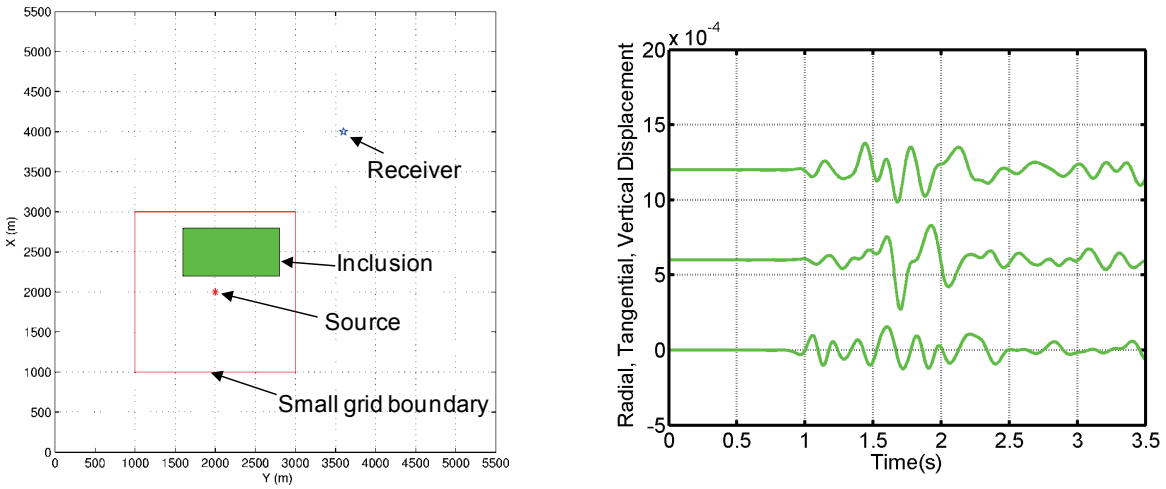

Figure 5. 3D representation theorem test case using CRAM3D with a full nonlinear material model and a 0.5 KT explosion. Initial cavity radius is 5m, which expands to 10.4m. The nonlinear region extends to about 90m. Nonlinear deformation increases the amplitude by about a factor of 6 relative to the linear model (Figure 3). The tangential component is increased more than the vertical and radial.

Figure 6 shows the regions of nonlinear deformation of four 3D nonlinear calculations for a 5 kiloton explosion at 102 meters depth in a half space of Degelen (nonlinear) granite overlain by a shallow linear layer (30m). Calculations were performed for the following four cases: the homogenous (two homogenous layers) medium, a heterogeneous medium with two buried low velocity elastic inclusions, a medium with topography, and a medium with weaker (lower strength) granite on one side of the calculation. In the latter, the weak structure reaches the surface. The heterogeneous model is implemented with homogenous elastic blocks with no nonlinear deformation. The topographic model is implemented with a Gaussian-hill with a peak of 6m, located off the epicenter. Gravity is included in all calculations.

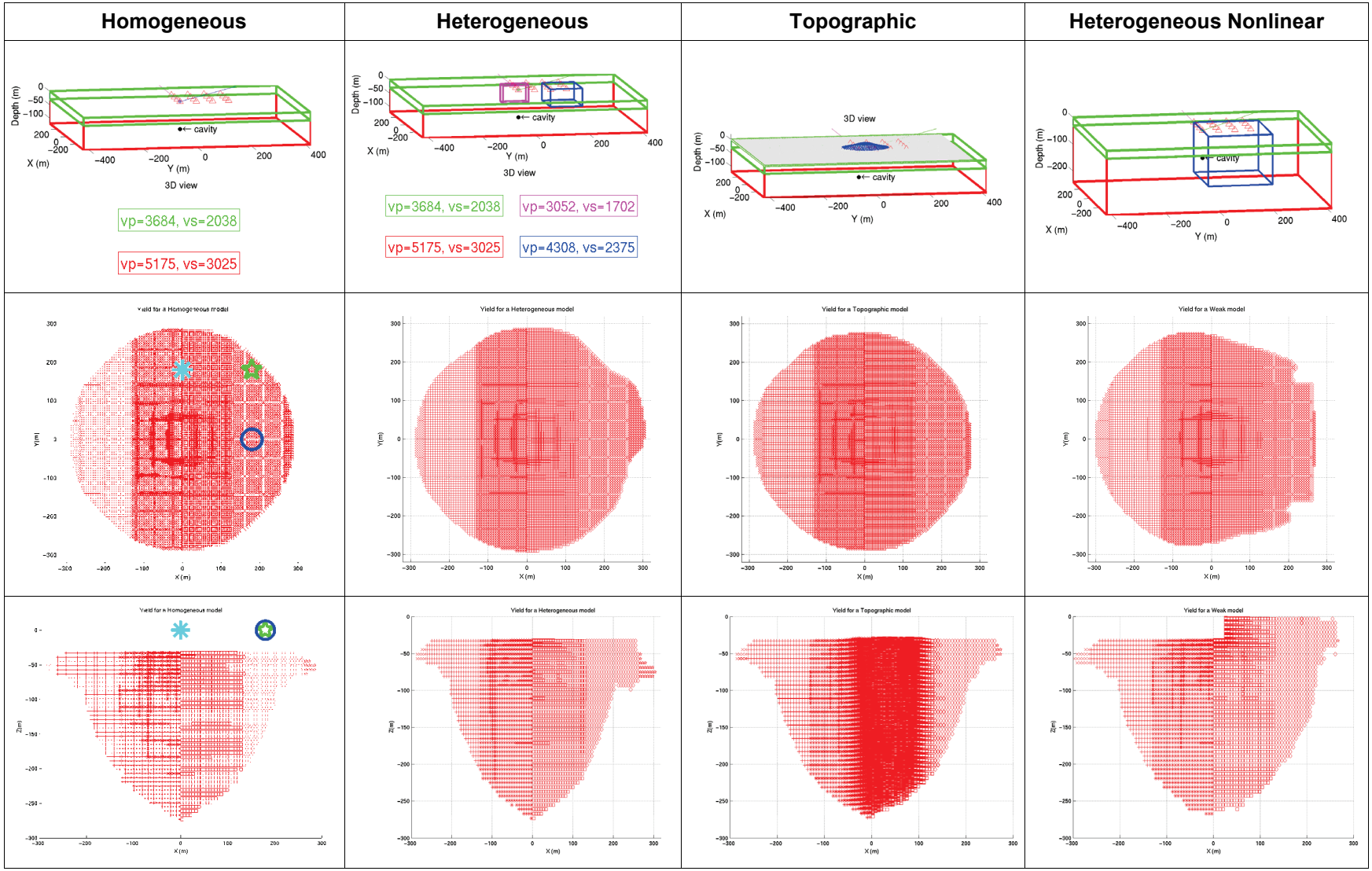

Figure 6. 3D nonlinear calculations for (left to right) a plane-layered structure, a structure with two elastic inclusions within the nonlinear region, a structure with a topographic hill near the explosion, and a plane layered structure with a nonlinear heterogeneity (weakened granite) on one side of the explosion (5 kt). Top row shows the models, the middle row shows a map view of the extent of nonlinear yielding, and the bottom row a cross-section view of the nonlinear region for each calculation. Marks are the location of seismograms shown in Figure 7.

Waveforms from the calculations illustrated in Figure 6 are shown in Figure 7. Note that each of the heterogeneous cases exhibits a substantial tangential component waveform that does not exist in the homogeneous case.

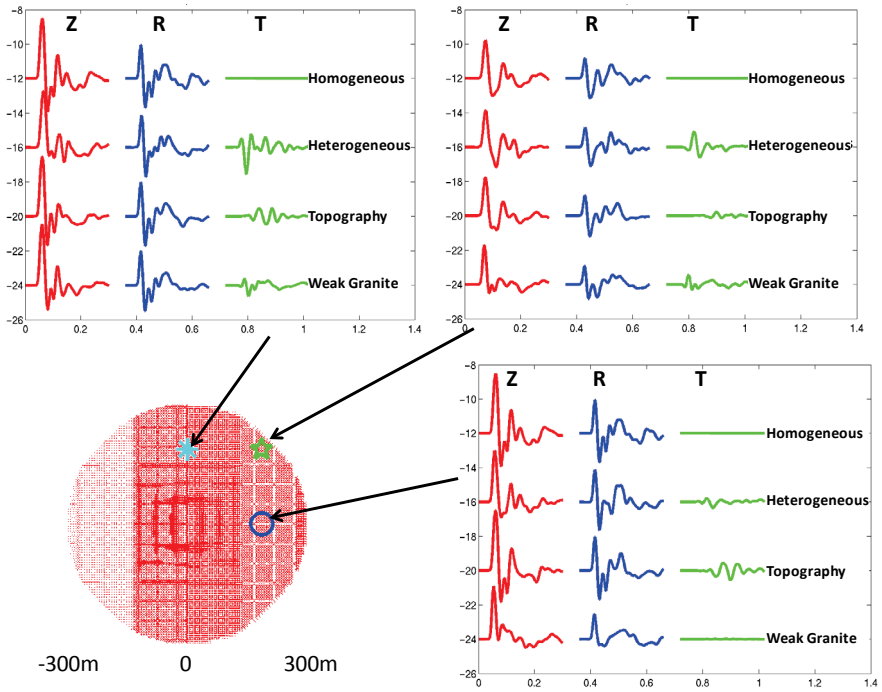

Figure 7. Vertical (red), radial (blue) and tangential (green) waveforms on the free surface at the points indicated by the arrows for the four 5 KT calculations shown in Figure 6.

Tensile Failure

Tensile cracks are calculated using algorithms from Maenchen and Sack (1964) in which crack strains are computed from the applied principal stresses. When the tensile stress exceeds the material's tensile strength, a crack forms normal to the direction of this stress. The 2D algorithms are extended into 3D and the solutions are compared for a spherical cavity in Figure 8. There is good agreement between the solutions at two surface locations 60m and 120m from the epicenter in 2D (red curve) and 3D (blue), demonstrating correct implementation of the crack algorithms extended from 2D to 3D. It also shows that the amplitudes with tensile cracking are higher than without tensile cracking (green curves) due to weakening. Figure 9 shows the tensile crack distributions in 2D and 3D. Both show initiation of tensile cracks near the free surface due to spall and tensile cracks near the pressurized cavity.

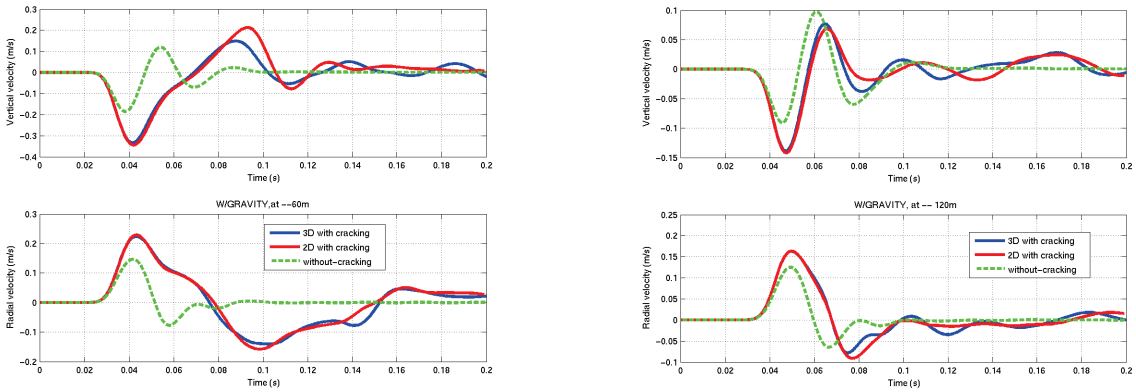

Figure 8. Vertical (top) and Radial (bottom) velocity at the surface at stations 60m (left) and 120m (right) from the point above the explosion. With cracking the velocity at 60m clearly shows evidence of spall as indicated by constant acceleration from 0.04 to 0.10 s. Blue and red curves are 3D and 2D calculations, respectively, with cracking, and the green curve is without. Note the good agreement between the solutions with tensile cracks in 2D and 3D.

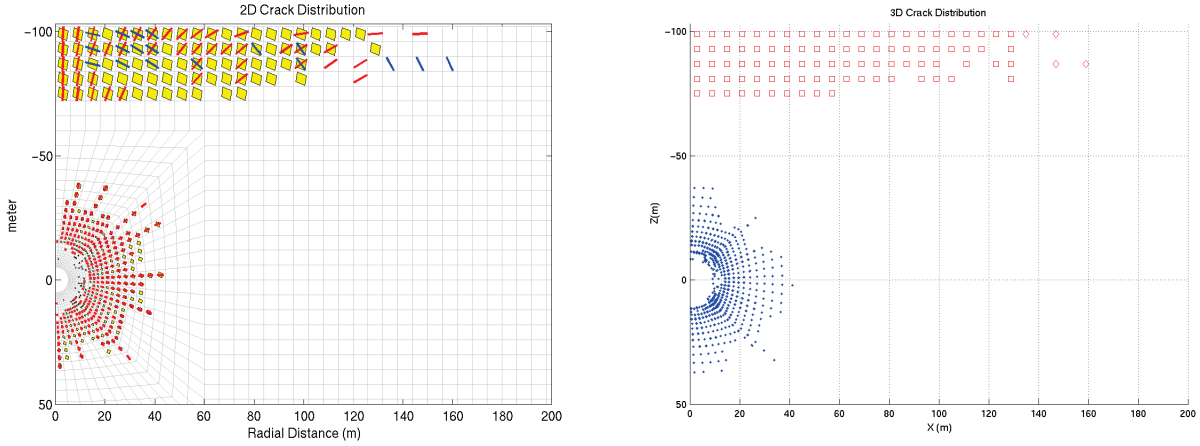

Figure 9. Crack distribution comparisons. Left: 2D crack distribution (symbols indicate the crack opening surfaces); Right: 3D crack distribution in a vertical cross section in which blue symbols indicate the cracks in the inner grid and red squares mark the cracks in the outer grid.

Far Field Propagation of 3D Calculations

Earlier we showed how the representation theorem is used to propagate 3D calculations and showed a full waveform example in the local distance range. Figure 10 shows far-field body waves from two 0.2-kiloton nonlinear calculations: the background structure and the structure with the weak inclusion. The weak rock causes a small amplitude increase in the far-field *P* wave, and otherwise the *P* waves are very similar. However, the heterogeneity causes a substantial *SH* wave to be generated, about 1/3 the size of the direct *P*-wave, which is absent in the background structure. The waveforms in Figure 10 were calculated for a 20º from vertical takeoff angle at an azimuth of 64º. They are broadband waveforms, and so are narrower than observed through typical short-period instruments which filter out the higher frequencies.

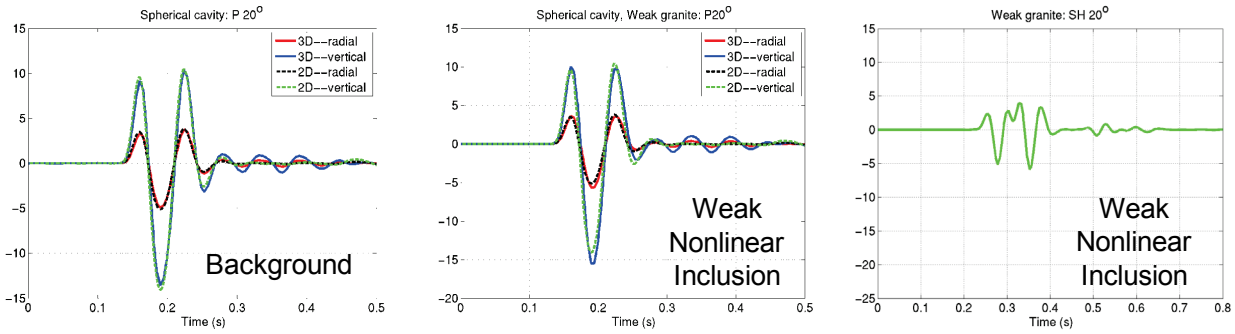

Figure 10. Far field body waves from two 3D nonlinear calculations. Left: *P* waves from the background structure. Middle: *P* waves from the structure with a weak nonlinear inclusion. Right: *SH* waves from the structure with a weak nonlinear inclusion. *P* waves from a 2D axisymmetric calculation in the background structure are shown for comparison on the left and middle figures.

Although the full waveform Green's function generates the entire waveform, the far-field body wave and modal Green's functions are also very useful for gaining insight into the explosion source. The waveforms in Figure 10, for example, are very simple compared to regional full-waveform seismograms and so allow us to distinguish source from propagation effects. Modal Green's functions allow us to separate the fundamental model and higher mode surface waves that are generated at the source.

For a full waveform example at a distance of 650km, we calculate a 5 kt explosion at a depth of 402m in the Degelen structure. The structure layout is similar to the heterogeneous nonlinear structure in Figure 6. The heterogeneous material is weaker than it surroundings. In this calculation, both shear failure and tensile failure are included. Figure 11 shows the nonlinear shear failure extent (top plots) and tensile failure extent (bottom plots) in

the horizontal and vertical views. This demonstrates the asymmetry in nonlinear deformation about the Y axis due to the weak material with symmetry about the X axis. The three rays (blue, green and black) denote the directions of the far field receivers at which the full waveforms are calculated.

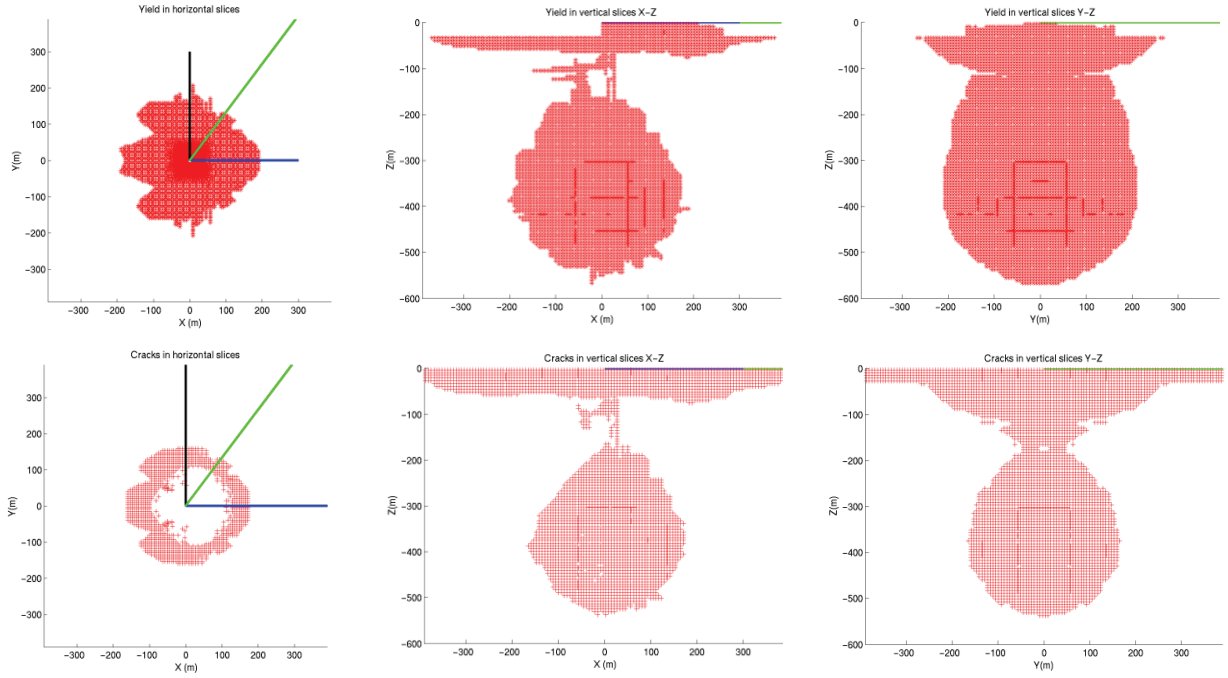

Figure 11. Top: Nonlinear yield extent of a 5 kt explosion. Horizontal and vertical slices are shown from left to right. Bottom: tensile failure. Horizontal slices are at shot level. Note the significant asymmetry about Y of the nonlinear deformation region due to the heterogeneity.

Figure 12 shows these waveforms at 650km. The left, middle and right locations correspond to the directions, black, green and blue, indicated in Figure 11. Each plot shows the radial (red), tangential (green) and vertical components (blue). Due to the heterogeneity and resulting nonlinear deformation asymmetry, these waveforms show significant tangential components for the location on the Y axis although the radial and vertical components show little variations in different directions. The results are consistent with those solutions from a symmetric explosion plus non-zero off diagonal moment components, resulting from the contrast between the weak materials and the adjacent strong Degelen material.

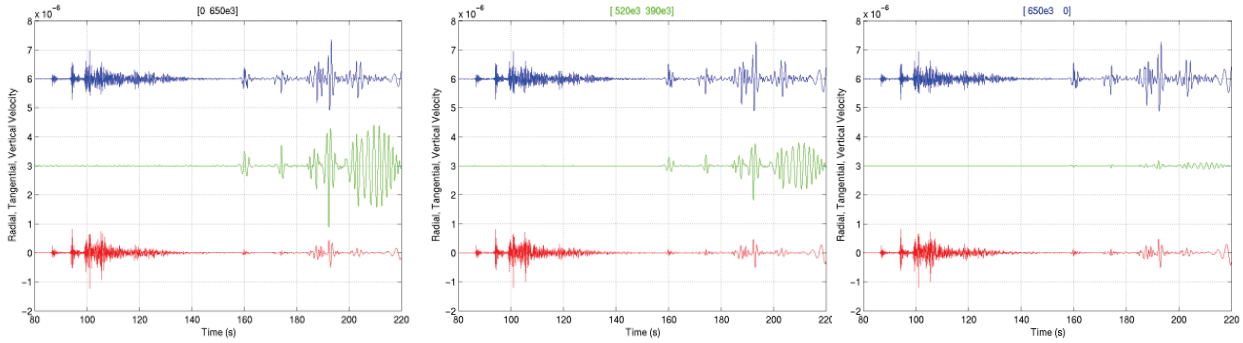

Figure 12. Full waveforms at 650km in the three directions indicated in Figure 11. The left one corresponds to the black line and yields a significant tangential component. The middle corresponds to the green line and the tangential component is reduced. The right one corresponds to the blue line in the symmetry plane so has little tangential component.

CONCLUSIONS AND RECOMMENDATIONS

We have completed development of a 3D version of CRAM, the Lagrangian code used previously for performing axisymmetric calculations of underground explosions. The code includes a tensile crack model and gravity, as well as all of the material models contained in axisymmetric CRAM. We have implemented a procedure for propagating the results of 3D source region calculations to regional and teleseismic distances using the representation theorem to couple source region calculations to wavenumber integration, modal and far-field body wave codes.

Our plans for the remainder of the project are to complete testing of the numerical methods and then perform 3D calculations designed to understand and model the effects of 3D source region heterogeneity and the seismic response to that heterogeneity.

REFERENCES

Apsel, R. J. and J. E. Luco (1983). On the Green's Functions for a Layered Half-Space, Part II, *Bull. Seismol. Soc. Am*. 73: pp. 931–951.

Bache, T. C. and D. G. Harkrider (1976). The Body Waves Due to a General Seismic source in a Layered Earth Model, *Bull. Seismol. Soc. Am*. 66: 1805–1819.

Bache, T. C., S. M. Day and H. J. Swanger (1982), Rayleigh Wave Synthetic Seismograms from Multi-Dimensional Simulations of Underground Explosions, *Bull. Seismol. Soc. Am*. 72: 15–28.

Fisk, M. D. (2006). Source spectral modeling of regional P/S discriminants at nuclear test sites in China and the former Soviet Union, *Bull. Seismol. Soc. Am*. 96: 2348–2367.

Fisk, M. D. (2007). Corner frequency scaling of regional seismic phases for underground nuclear explosions at the Nevada test site, *Bull. Seismol. Soc. Am*. 97: 977–988.

Luco, J. E. and R. J. Apsel (1983). On the Green's Functions for a Layered Half-Space, Part I, *Bull. Seismol. Soc. Am*. 73: 909–929.

Maenchen, G. and S. Sack (1964). The tensor code, in *Methods in Computational Physics*, Vol 3, edited by Berni Alder, 181–210.

Murphy, J. R., B. W. Barker, D. D. Sultanov, and O. P. Kuznetsov (2009). S-Wave Generation by Underground Explosions: Implications from Observed Frequency-Dependent Source Scaling, *Bull. Seismol. Soc. Am.* 99: 809–829, doi: 10.1785/0120080126.

Stevens, J. L., T. G. Barker, S. M. Day, K. L. McLaughlin, N. Rimer, and B. Shkoller (1991). Simulation of teleseismic body waves, regional seismograms, and Rayleigh wave phase shifts using two-dimensional nonlinear models of explosion sources, AGU Geophysical Monograph 65: Explosion Source Phenomenology, S. Taylor, H. Patton, P. Richards, editors, ISBN 0-87590-031-3, 239–252.

Stevens, J. L., N. Rimer, H. Xu, G. E. Baker and S. M. Day (2003). Near field and regional modeling of explosions at the Degelen Test Site, SAIC final report to DTRA, SAIC-02/2050, January.

Stevens, J. L., G. E. Baker, H. Xu, T. J. Bennett, N. Rimer and S. M. Day (2004). The Physical Basis of Lg Generation by Explosion Sources, SAIC Final Report submitted to the National Nuclear Security Administration under contract DE-FC03-02SF22676, December.

Stevens, J. L., S. Gibbons, N. Rimer, H. Xu, C. Lindholm, F. Ringdal, T. Kvaerna, and J. R. Murphy (2006). Analysis and simulation of chemical explosions in nonspherical cavities in granite, *J. Geophys. Res*., 111, B04306, doi:10.1029/2005JB003768.

Stevens, J. L. and G. E. Baker (2009). Seismic wave generation by a non-isotropic explosion source, *J. Geophys. Res.* 114: B12302, doi:10.1029/2008JB005965.

Stevens, Jeffry L. and Heming Xu (2009). Wave propagation from complex 3D sources using the representation theorem, in *Proceedings of the 2009 Monitoring Research Review: Ground-Based Nuclear Explosion Monitoring Technologies*, LA-UR-09-05276, Vol. 1, pp. 574–581.

Weart, Wendell D. (1965). VELA UNIFORM, Project SHOAL, Project 1.1, Free Field Earth Motion and Spalling Measurements in Granite, Sandia Corporation final report VUF-2001 to the Advanced Research Projects Agency, February.

Zhou, L. and D. G. Harkrider (1992). Wave fields from an off-center explosion in an embedded solid sphere, *Bull. Seismol. Soc. Am*. 82: 1927–1955.